Journal of Biomedical Optics 9(5), 982–994 (September/October 2004)

Measuring red blood cell flow dynamics in a glass capillary using Doppler optical coherence tomography and Doppler amplitude optical coherence tomography

Julian Moger
Stephen J. Matcher
C. Peter Winlove
University of Exeter
Biomedical Physics Group
Exeter, EX4 4QL, United Kingdom

Angela Shore
Peninsular Medical School
Plymouth, PL6 8BX, United Kingdom
E-mail: J.Moger@Exeter.ac.uk

Abstract. Blood, being a suspension of deformable red cells suspended in plasma, displays flow dynamics considerably more complicated than those of an ideal Newtonian fluid. Flow dynamics in blood capillaries of a few hundred micrometers in diameter are investigated using Doppler optical coherence tomography (DOCT) and Doppler amplitude optical coherence tomography (DAOCT), a novel extension of DOCT. Velocity profiles and concentration distributions of normal and rigidified *in vitro* red blood cell suspensions are shown to vary as functions of mean flow velocity, cell concentration, and cell rigidity. Deviation from the parabolic velocity profile expected for Pouseille flow is observed for both rigid and normal cells at low flow rates. Axial red cell migration both toward and away from the tube axis is observed for both rigid and normal cells as a function of flow velocity. Good agreement is found between our measurements, and theoretical expectations.
[DOI: 10.1117/1.1781163]

Keywords: Doppler optical coherence tomography; red blood cell velocity profile.

Paper 03079 received Jun. 17, 2003; revised manuscript received Oct. 30, 2003; accepted for publication Feb. 16, 2004.

1 Introduction

Detailed knowledge of flow dynamics in blood vessels is important for several reasons. First, transport of nutrients from blood to tissue is influenced by the blood flow velocity profile and particle distribution over the vessel cross section. Second, to estimate the volume flow rate and effective hematocrit through small vessels a parabolic velocity profile is often assumed.[1] This approach will lead to errors if the flow profile is flattened or plug like. Third, accurate measurement of flow profiles provides useful information about shear rates in the fluid and at the vessel wall. Shear forces at the vessel wall are a potent mediator of vasodilation, as they stimulate the release of nitric oxide by the endothelial cells.

Although many publications on the flow dynamics of blood in small vessels exist, many have yielded conflicting results. The majority of these studies rely predominantly on data collected using video microscopy, a technique in which the velocity of particles in the blood is calculated by measuring the distance a particle moves between video frames.

Velocity profiles of whole blood have been obtained *in vivo* using platelets as small natural markers of flow.[2] Although it has been demonstrated that this technique can be used in vessels with diameters as small as 17 μm, a great deal of time-consuming averaging and analysis is required to produce reliable velocity profiles.

Far less work has been published on the radial distributions of the blood cells caused by the shear forces that arise in a moving fluid. To achieve an accurate representation of the cell distribution the axial position of many blood cells is required. The positions of the small natural markers used to measure flow in whole blood do not necessarily bear any relation to the spatial distribution of the blood cells that are of interest. Small concentrations of ghost cells, red blood cells with the hemoglobin removed, are often added to whole blood as *in vitro* markers to give a semidirect measure of red blood cell position. Although ghost cells are widely used in video microscopy to investigate blood flow dynamics, the process of analyzing the axial positions of a sufficient number of ghosts cells is time consuming and tedious. In addition, removal of the hemoglobin causes the mechanical properties of the ghost cells to differ from those of a normal red blood cell; this will affect the way in which they interact with the solution, hence giving a false representation of the axial distribution of cells.

Other techniques commonly used for measuring blood flow velocity, such as laser Doppler flowmetry (LDF) and photon correlation velocimetry are not intrinsically depth-resolved. Doppler low-coherence techniques such as Doppler optical coherence tomography (DOCT) can offer direct measurement of the velocity profile *in vitro* and *in vivo* with a high degree of spatial resolution. The concept of measuring relative red cell concentrations by calculating the spectral density has been widely used[3] in LDF. Doppler amplitude

Address all correspondence to Julian Moger. University of Exeter, Biomedical Physics Group, Exeter EX4 4QL, United Kingdom. Tel: 441392 264118; Fax: 441392 264111; E-mail J.Moger@Exeter.ac.uk

1083-3668/2004/$15.00 © 2004 SPIE

OCT (DAOCT) uses a similar principle to give corresponding information on the cross-sectional concentration distribution of the red cells with high spatial resolution. This investigation demonstrates the effectiveness of DOCT and DAOCT as tools for probing the flow dynamics of red blood cells in a small capillary *in vitro*.

1.1 *Blood Flow Dynamics in Small Vessels*

To understand blood flow dynamics in small vessels one must consider the particulate nature of blood. The concentration of red cells in whole blood is far greater than any other formed elements, and therefore dominates the flow characteristics of whole blood.

1.1.1 *Flow profiles*

When the concentration of particles in the flowing suspension exceeds 0.5% by volume, experiments have shown that particle-to-particle interactions or near collisions occur. These progressively alter the particle motion and hence velocity profile.

To understand the behavior of concentrated suspensions it is necessary to consider both the concentration c of the suspension and the particle size relative to the tube diameter d/D, where d and D are the particle and tube diameters, respectively.

If relatively small particles are present in a solution at concentration less than 5%, the velocity profile is close to parabolic. As the relative particle radius or concentration is increased, the velocity profile becomes progressively blunted. The degree of blunting is influenced by the particle rigidity; flexible or fluid particles of the same concentration and size relative to the tube diameter show less blunting than rigid particles. This difference in behavior is summarized in Fig. 1 (adapted from Caro et al.[4]). In the top figure, rigid and flexible spheres of the same size are compared to rigid spheres of half the diameter in solution at 30% concentration by volume. We can see that at this concentration the velocity profile of the large rigid spheres is flat, and the region of ''plug flow,'' in which all spheres move with uniform velocity in the direction of flow, extends almost the whole diameter of the tube almost to the tube wall. Smaller rigid spheres do not show such a wide zone of plug flow in the core. When rigid behavior is compared with that of the fluid drops, it can be seen that large fluid drops exhibit less blunting than rigid spheres of half their diameter.

In the case of rigid particles, the velocity profile is determined solely by the particle concentration and relative radius, and is independent of the fluid flow rate.[3] In contrast, the velocity profile for liquid drops is affected by flow rate, with the degree of blunting decreasing as the flow rate is increased.

The lower part of Fig. 1 compares flow velocity profiles for ghost red blood cells and rigid disks of the same size and concentration. The velocity profile of the rigid disks has a wider region of plug flow than the red blood cells at the same velocity. The red blood cell suspension also shows how increasing the flow rate causes the region of plug flow to decrease. At very high flow rates the velocity profile is almost parabolic.

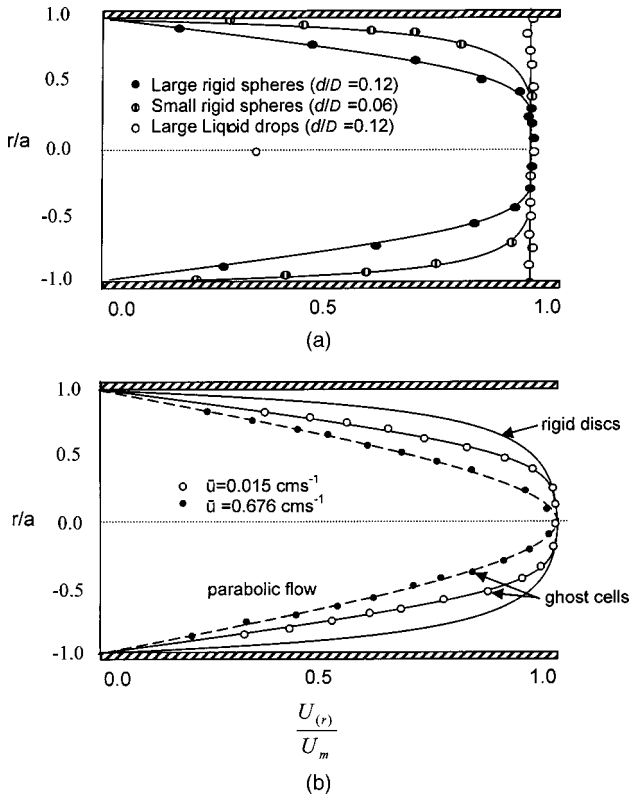

Fig. 1 Velocity profiles at very low Reynolds numbers in straight tubes for particles suspensions and ghost red cells. Local velocities $[U(r)]$ are plotted as ratios of the center line velocity u_m; this means that profiles are scaled so that center-line velocity is unity in all cases. Velocity profiles for (a) the same concentrations of (1) large ($d/D=0.12$), (2) small ($d/D=0.06$) liquid drops, and (3) large rigid spheres ($d/D=0.12$), and (b) for suspensions of ghost red cells and rigid disks of approximately the same size and concentration. The profiles for the ghost cells are shown at two different flow rates. Adapted from Caro et al.[4]

1.1.2 *Particle distribution*

At higher flow rates, inertial forces of the fluid become important. The underlying mechanisms controlling particle motion are complex and involve both the inertia of the fluid and the interaction of the particle with the tube wall.

Deformable bodies exhibit radial migration toward the center of the tube; rigid particles also migrate, although not always toward the center. The behavior of rigid particles under these conditions is known as the ''tubular-pinch'' effect.[3] Particles initially near the tube wall move toward the axis, while particles initially near the axis move toward the tube walls. Equilibrium is reached when all the particles occupy the radial position of $0.6r$, where r is the internal radius of the tube. Migration velocity depends on the radial position and decreases as the equilibrium location is approached; the radial velocity increases with Reynolds number and as the particle size increases relative to the tube diameter.

The types of motion observed for rigid and deformable particles are summarized in Fig. 2. Except for rigid particles at very low flow-rates, there is always particle migration away from the tube walls.

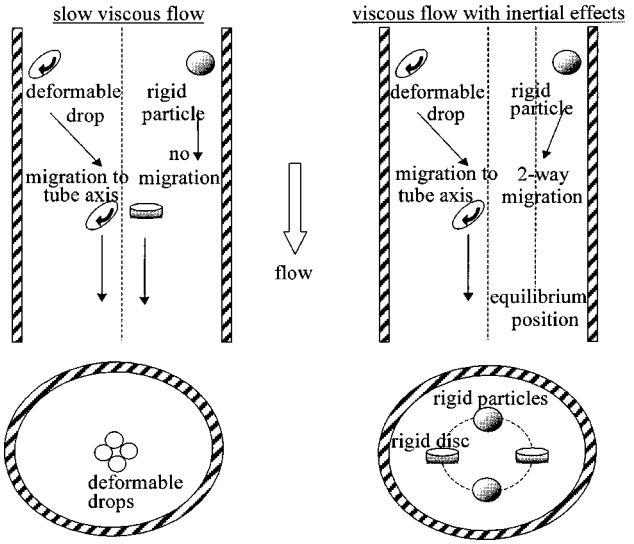

Fig. 2 Schematic of the differences in migration of rigid and deformable particles, on the left at low flow rate and on the right at a significantly higher flow rate. Adapted from Caro et al.[4]

The motion of red blood cells in plasma reflects both rigid and deformable particle behavior. When the flow rate is low enough for the shear rate in the vicinity of the red blood cells to be less than approximately 20 s^{-1}, the cell is seen to rotate like a rigid disk, retaining its biconcave shape. The flipping and periodicity of rotation are just as predicted for a rigid disk of the same diameter.

At shear rates greater than 20 s^{-1}, the behavior of the normal red blood cell progressively deviates from that of the rigid disk.

At shear rates greater than 1000 s^{-1} measurements of cell dimensions indicate that it has become deformed, but the characteristic biconcave shape is retained. At these high shear rates, axial migration from the wall is also observed and the migration velocity increases with shear-rate.

At very high shear rates, above 5000 s^{-1}, single red blood cells experience the tubular pinch effect, but with an equilibrium position nearer to the axis than that observed for rigid disks.

At shear rates less than around 2 s^{-1}, the red cells aggregate to form rod like structures called rouleaux; these show strong axial migration toward the center of the tube. As the shear rate is increased the rouleaux are broken down and become shorter, reducing the axial migration velocity. Studies on red blood cells hardened with glutaraldehyde show behavior close to that of the rigid disk and do not exhibit axial migration until the shear-rate is high enough for tubular pinch to occur.

2 Theory

In this study, we investigated the ability of DOCT to reveal these subtle changes in flow dynamics on whole blood and suspensions of normal and rigidified red cells, without the need for fluorescent labeling or the use of natural markers.

DOCT is a functional extension of optical coherence tomography (OCT) that uses motion (flow) in a sample as a source of contrast.[5–7] *In vitro* imaging of flow has been widely reported in tissue phantoms, while *in vivo* flow images have been demonstrated in animal models[8–10] and, more recently, in humans.

OCT and DOCT are based on low-coherence interferometry, using a Michelson interferometer with a broadbandwidth laser source. Light from the sample arm of the interferometer focused by a low-numerical-aperture lens penetrates the sample and is backscattered from various depths with amplitude depending on the local reflectivity of the sample. The reference arm length is varied either by a moving mirror or, more conveniently, using a high-speed Fourier-domain delay line.[11] The light beams backscattered from the

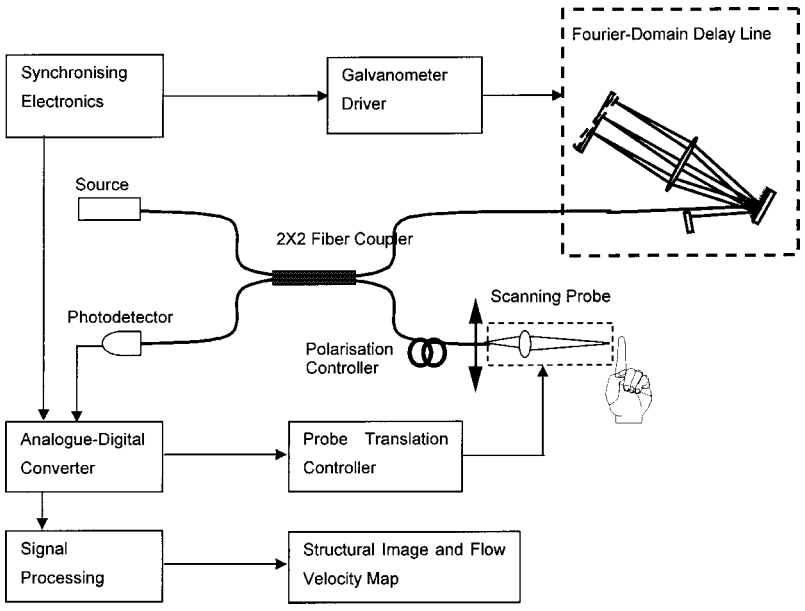

Fig. 3 Schematic of the DOCT system and signal processing apparatus.

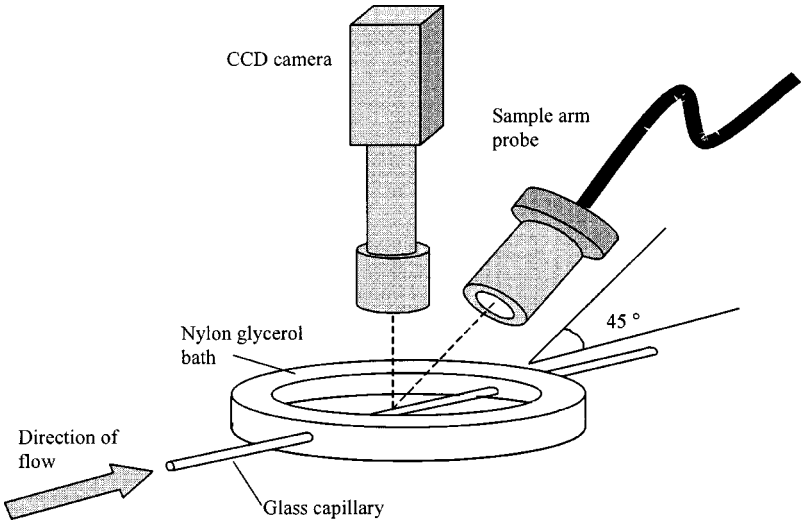

Fig. 4 Experimental flow phantom, indicating the relative alignment of the DOCT probe and CCD camera (not to scale).

sample and reference arms of the interferometer are recombined and directed to a photodetector. Sample light that is path-length-matched to within the source coherence length with light from the reference arm produces an interference signal, whose amplitude is proportional to the square root of the depth-resolved backscatter efficiency within the sample. The light returning from the reference arm is Doppler shifted by frequency $f_r = 2V_r/\lambda_0$, where V_r is the phase velocity generated by the moving mirror or delay line, and λ_0 is the center wavelength of the light source. Backscattered light from the reference and sample arms interfere to produce an interferometric signal, or interferogram. The amplitude of the interferogram is proportional to the square root of the light intensity returning from the sample, and the carrier frequency corresponds to the reference arm Doppler shift frequency f_r.

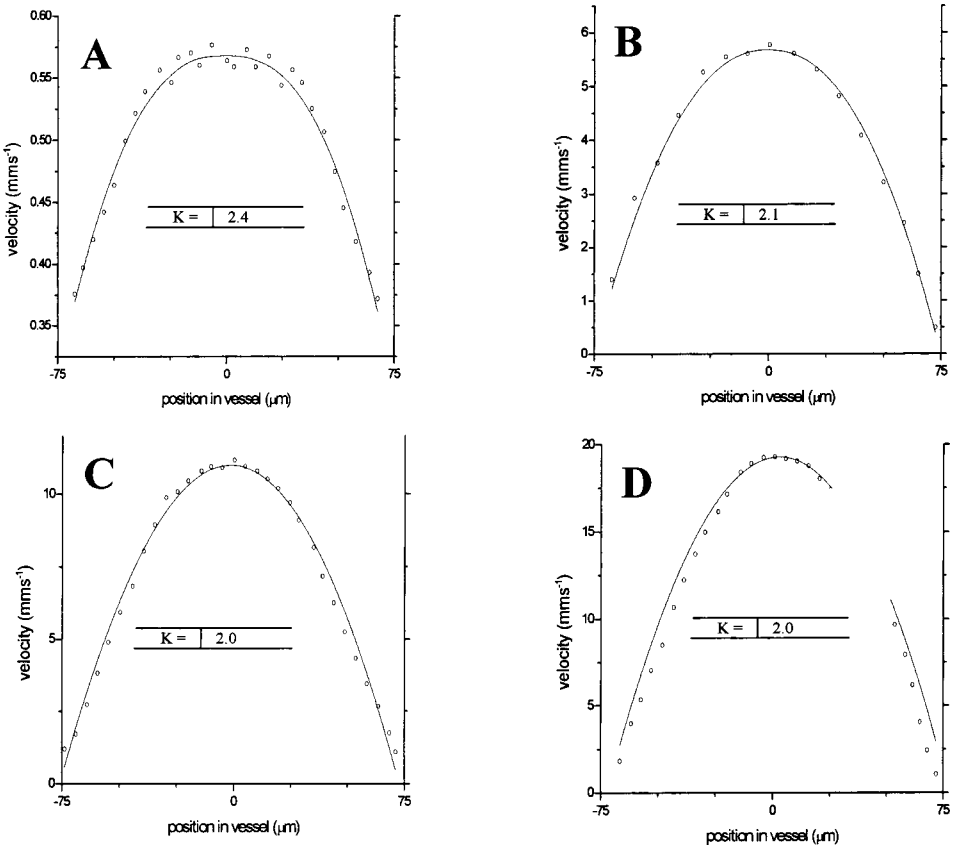

Fig. 5 Velocity profiles of normal RBCs in solution 40% by volume at four velocities: (a) 0.5, (b) 6, (c) 12, and (d) 20 mm/s.

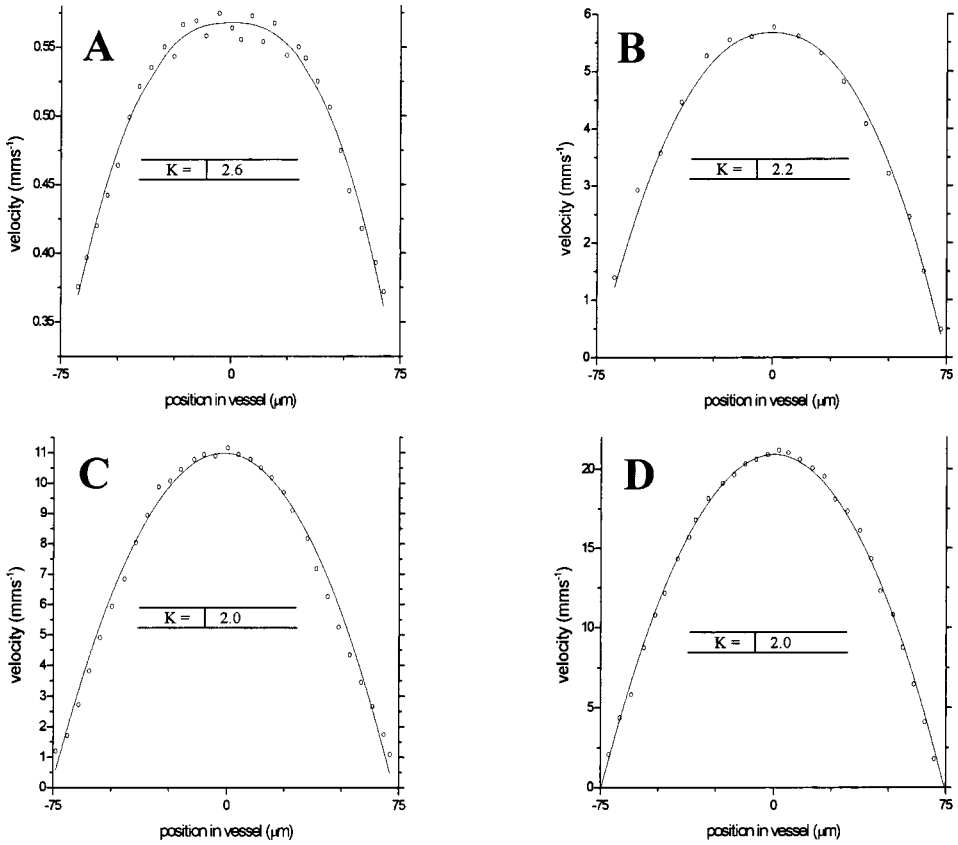

Fig. 6 Velocity profiles of fixed RBCs in solution 40% by volume at four velocities: (a) 0.5, (b) 6, (c) 12, and (d) 20 mm/s.

The contrast of an OCT image is derived from the amplitude of interferometric signal demodulated at the reference frequency f_r. If the sample contains moving scatters, i.e., red blood cells, then the carrier of the interferometric signal is Doppler shifted by frequency $f_s = 2V_s n_s \cos\theta/\lambda_0$, where V_s is velocity of the moving scatterer, n_s is the local refractive index of the sample, and θ is the angle of the direction of flow with respect to the sample beam. Therefore, areas of the sample containing flowing particles, such as blood vessels, appear empty or very low in intensity because the backscattered signal from the moving particles has been Doppler shifted away from the demodulation frequency f_r. This means that information on the density of flowing scatterers in a vessel is not retained. DOCT uses the frequency shift in the interferogram carrier frequency as a source of image contrast to generate a map of flow velocity, often using color to indicate flow direction.[7]

DAOCT is a functional extension of DOCT in which the image contrast is derived from the amplitude of the interferogram at the Doppler-shifted reference frequency[12] $(f_r + f_s)$. This source of contrast is sensitive to the density of scatterers rather than their velocity, and gives a useful additional parameter for characterizing flow distributions. The digitized interferometric signal is analyzed in software to find the peak in the interferogram, corresponding to the Doppler-shifted reference frequency; the squared amplitude of this peak is used as the image contrast.

3 Materials and Methods

OCT line scans were recorded through the center of a glass capillary to obtain the velocity profiles and spatial distribution of red blood cells as a function of their flow-rate within various fluid suspensions.

A schematic of the DOCT apparatus used in the experiments is illustrated in Fig. 3. The Michelson interferometer consists of a 2×2 fiber coupler that provides a stable interferogram with minimal interference from vibration and thermal air currents. Near-infrared light emitted by an amplified spontaneous emission (ASE) light source (B&W Tek, Inc.), with an optical output power of 7 mW, a center wavelength of 1550 nm, and a spectral full width half maximum of 100 nm was coupled into the source arm of the fiber coupler. The reference arm scanning was achieved by a Fourier-domain delay line,[10] which uses a diffraction grating and a galvanometer to generate an optical path difference of 1 to 2 mm with a maximum axial scan rate of 500 Hz. The sample arm probe, containing an objective lens with a numerical aperture of 0.12, yielding a lateral resolution of approximately 20 μm, was aligned at 45 deg to the long axis of a glass capillary, as shown in Fig. 4.

To reduce the signal caused by Fresnel reflection at the capillary walls it was set into a nylon bath and immersed in a refractive index-matching fluid (glycerol). A CCD camera, positioned directly above the capillary, was used to assist the

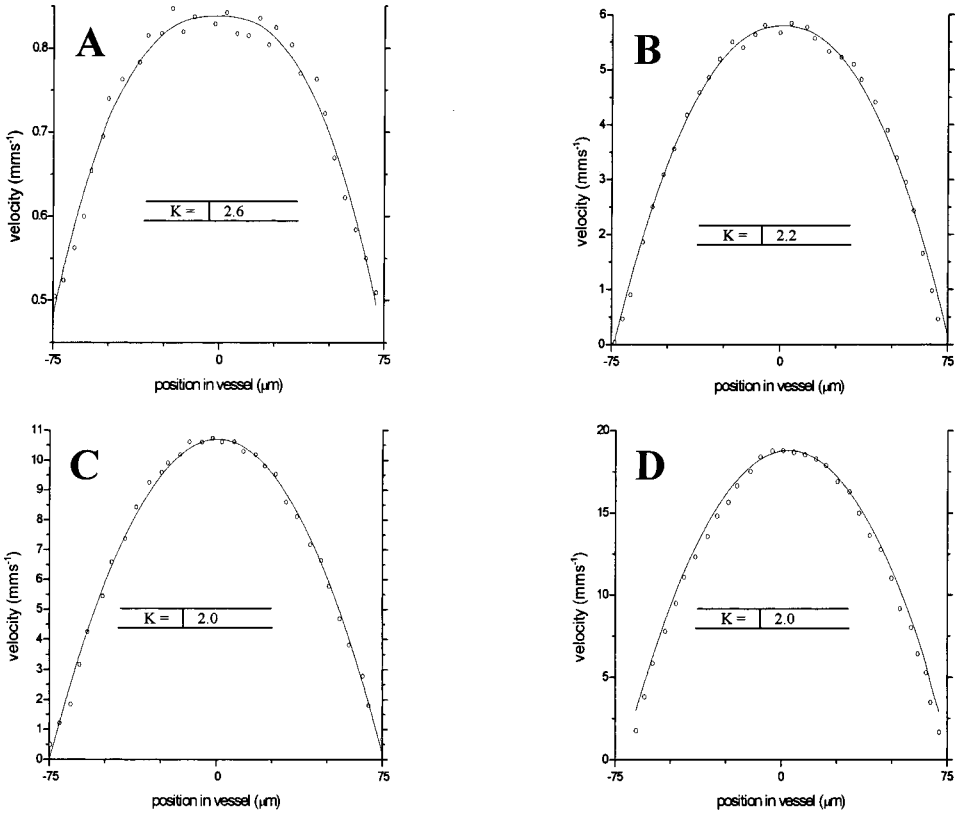

Fig. 7 Velocity profiles of normal RBCs in solution 60% by volume at four velocities: (a) 0.5, (b) 6, (c) 12, and (d) 20 mm/s.

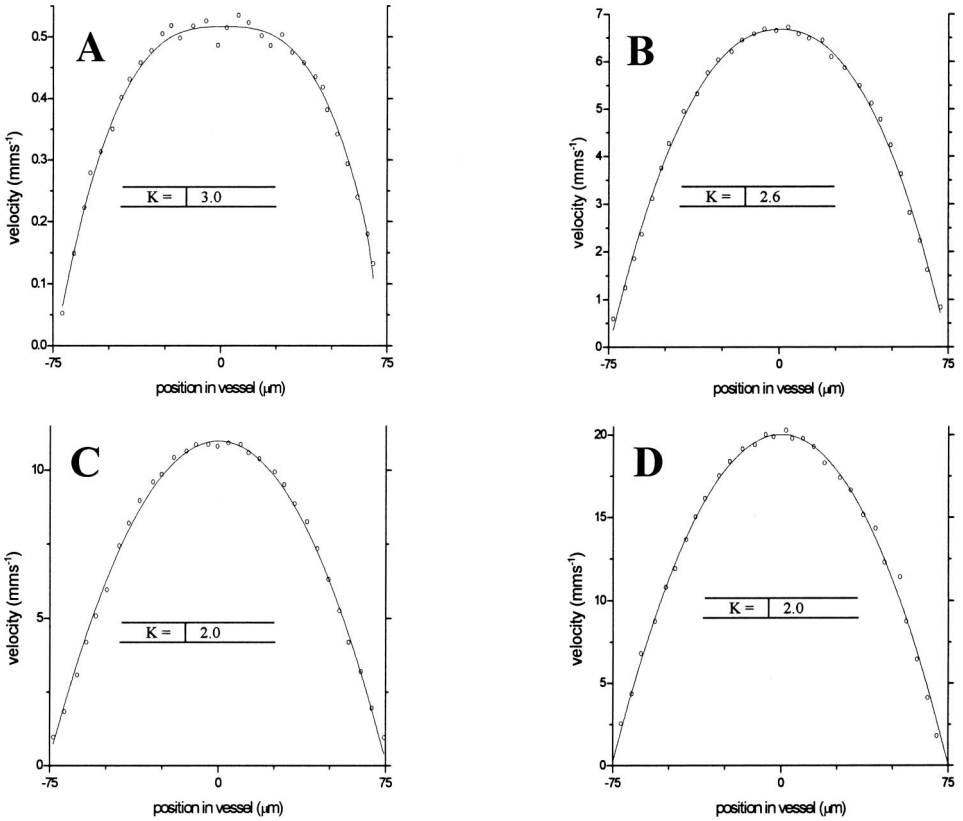

Fig. 8 Velocity profiles of fixed RBCs in solution 60% by volume at four velocities: (a) 0.5, (b) 6, (c) 12, and (d) 20 mm/s.

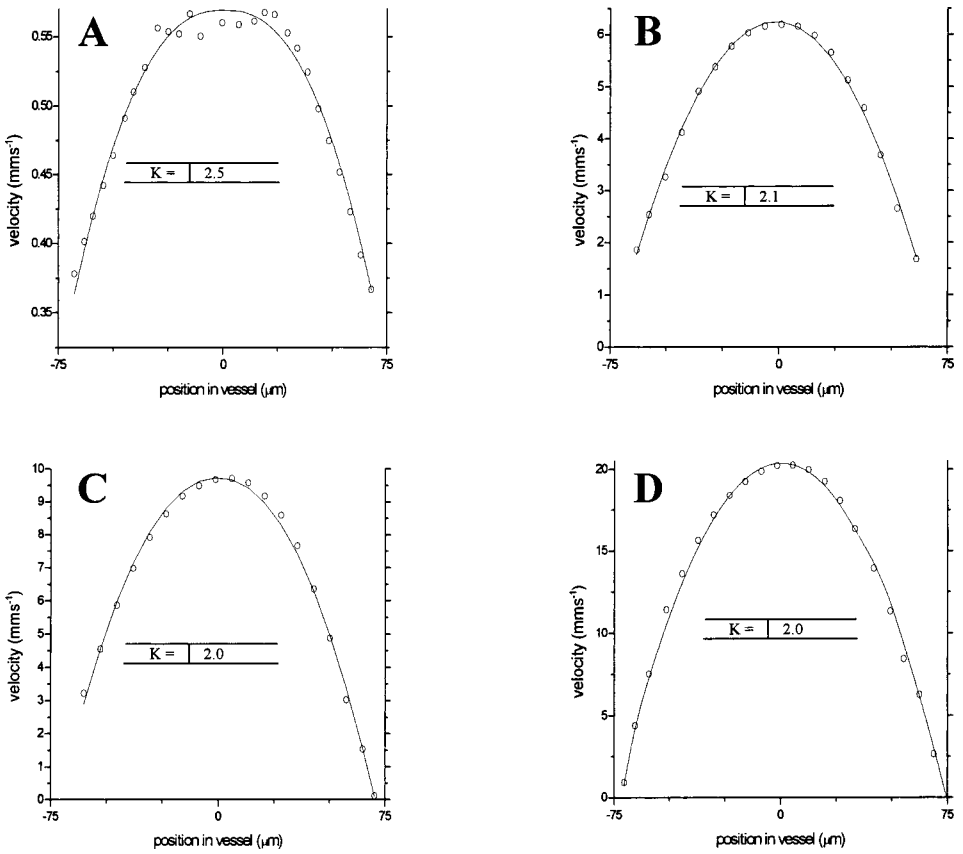

Fig. 9 Velocity profiles of RBCs in whole blood at four velocities: (a) 0.56, (b) 6, (c) 12, and (d) 20 mm/s.

alignment of the sample probe and the capillary. Blood cell suspensions were pumped through the capillary using an infusion pump to provide a constant flow rate. The capillary was mounted on an X-Y micrometer-driven translation stage to enable precise alignment of the capillary in the sample beam.

OCT line scans corresponding to a physical depth of 1 mm were acquired with a repetition rate of 5 Hz. Each line scan, consisting of 6400 points, was sample at 32 kHz and divided into 100 pixels, each of 64 data points in length. A spectrogram of each pixel was produced using a short-time Fourier transform algorithm,[7] producing a frequency bin separation corresponding to a velocity of approximately 1 mm s^{-1}.

Cross-sectional velocity profiles and red blood cell distributions were obtained by averaging DOCT and DAOCT line scans through the vertical axis of the capillary. Due to the highly forward scattering nature of red blood cells, and the consequently weak backscattered signal, line scans were averaged typically over several hundred line scans to improve the SNR; this also reduced the effect of any anomalous results caused by random motion in the solution. Care was taken to ensure the line scans were acquired through the vertical axis of the capillary. To do this, the CCD camera was adjusted until the probe beam, as visualized using a fluorescent card, intersected the plane of interest in the center of the CCD field of view. The capillary was then centered in the CCD video picture. Red blood cell (RBC) velocity profiles and concentration distributions were obtained for whole blood and suspensions of normal and rigid red blood cells at various concentrations and flow rates. To investigate the dependence of the velocity profiles and particle distribution on RBC deformability the experiments for normal suspensions of RBCs were repeated using cells made rigid by being fixed in formaldehyde.

Venous blood taken from healthy volunteers was used to make three suspensions of RBCs; whole blood, a suspension of RBCs in phosphate-buffered saline, and rigidified RBCs suspended in saline. To prevent the blood from coagulating during the experiment, heparin was added at 1% by volume. All experiments were carried out within a few hours of taking each sample. Heparinized whole blood was centrifuged at 3000 rpm for 10 min and the plasma and buffy coat were aspirated off. Phosphate buffered saline (pH 7.4) made from commercially available tablets (Sigma-Aldrich) was added to the remaining red cells in equal volume, and thoroughly mixed to rinse the red cells of any remaining unwanted white cells or plasma. The washing and centrifuging was repeated once. Phosphate-buffered saline (PBS) was then added to the remaining red cells to make up a suspension to the required concentration by volume.

A suspension of rigid red cells was prepared by mixing the required volumes of formaldehyde and RBC suspension in PBS to achieve a final concentration of 4% formaldehyde and the required volume ratio of RBCs.

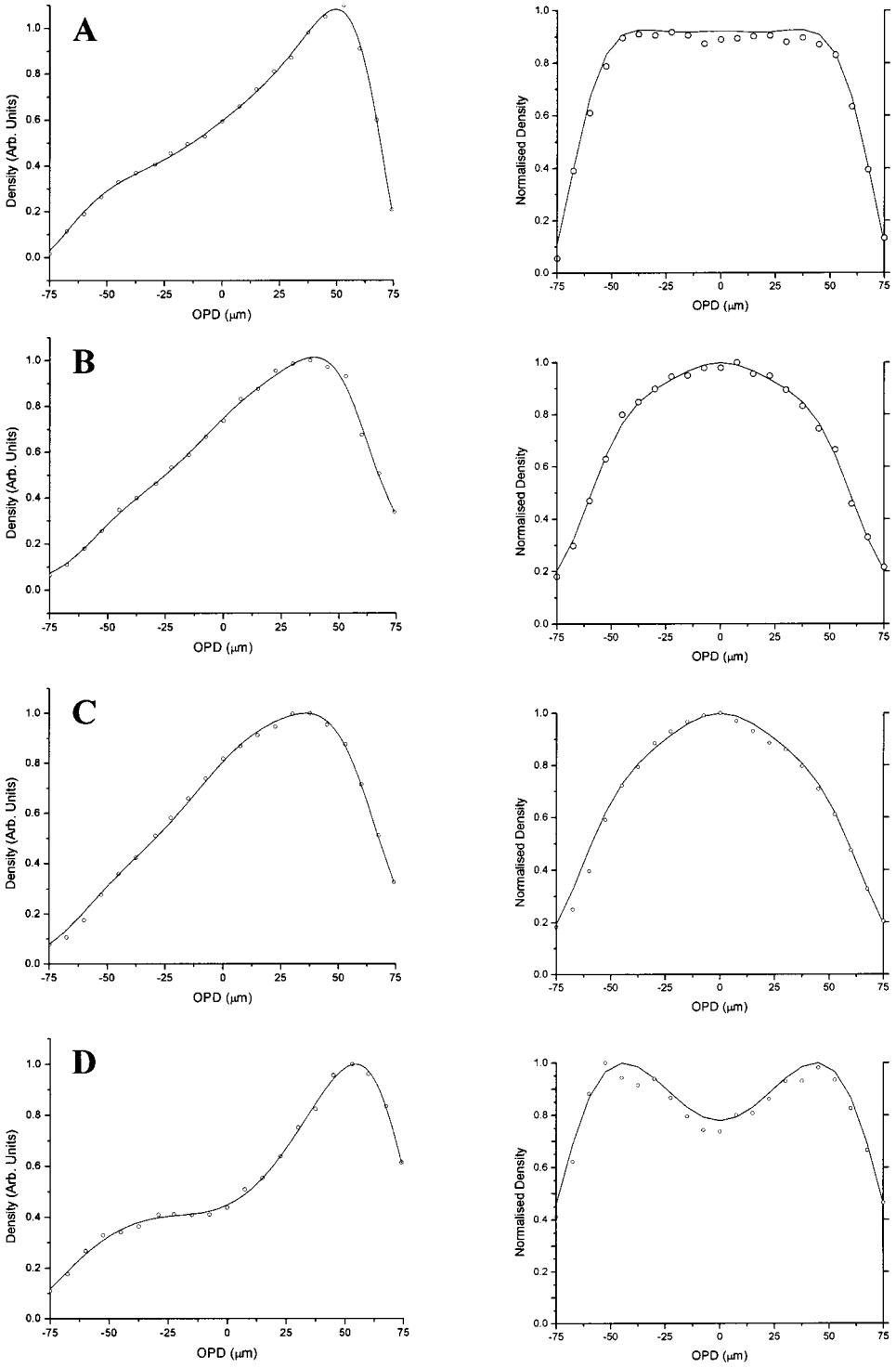

Fig. 10 Left-hand graphs show the raw data points for whole blood, obtained by averaging 1000 DAOCT line scans; the polynomial fitting function is shown as a dotted line. The attenuation corrected density distributions are shown on the right-hand side. The four distributions correspond to four flow velocities: (a) 0.5, (b) 6, (c) 12, and (d) 20 mm/s.

3.1 *Data Analysis*

This section describes the postacquisition data analysis and modeling procedure used to characterize the velocity profiles and cell concentration distributions of the different type of RBC suspensions.

3.1.1 *Velocity profiles*

Currently, several different theories exist to describe the flow dynamics in small tubes. All are semiempirical and no theory has been proposed that is derived from the basic properties of

Table 1 Summary of K values for the five RBC suspensions at approximate flow velocities of 0.5, 6.0, 11.0, and 21.0 mm s^{-1} with regression coefficients (chi-squared) and associated confidence level p included.

	0.5 mm s^{-1}			6.0 mm s^{-1}			11.0 mm s^{-1}			21.0 mm s^{-1}		
	K	χ^2	p	K	χ^2	p	K	χ^2	p	K	χ^2	p
Fixed 40%	2.6	15.6	92.6	2.2	12.9	97.7	2.0	11.1	99.2	2.0	8.5	99.9
Fixed 60%	3.0	15.9	91.8	2.6	13.2	97.4	2.0	11.9	98.7	2.0	8.9	99.9
Unfixed 40%	2.4	16.2	90.9	2.1	11.9	98.7	2.0	10.9	99.3	2.0	7.9	99.9
Unfixed 60%	2.6	14.0	96.1	2.2	11.1	99.2	2.0	10.1	99.6	2.0	7.2	99.9
Whole blood	2.5	16.9	89.0	2.1	12.0	98.6	2.0	10.6	99.4	2.0	8.4	99.9

blood cells and plasma.[1] To describe the shape of the experimental velocity profiles, the following equation was used.[2]

$$V(r)=V_{\max}\left[1-\left|a\left(\frac{r}{R}\right)+b\right|^{K}\right],\quad 0\leqslant\frac{r}{R}\leqslant 1,\quad a\geqslant 0, \tag{1}$$

where $V(r)$ is the velocity at radial position r, $V_{\max}$ is the velocity at the center of the tube, and R is the radius of the tube. Due to the nonslip condition at the tube wall, i.e., $V(R)=0$ and the finite spatial and velocity resolution of the system, data points near the tube wall tend to be unreliable. A scaling factor a is introduced to allow the model velocity profile to intercept zero at points other than $r=R$. Any asymmetry in the profiles was taken into account by parameter b, which corrects for a shift of the top of the profile away from the center of the tube. Due to the axial symmetry of the system, any such asymmetry can be considered as a measurement artifact, arising perhaps from asymmetric placement of the incident beam waist within the tube.

The shape of the profile is characterized by the parameter K, a value of $K=2$ corresponds to the parabolic velocity profile characteristic of Pouseille flow. The profile becomes progressively flatter as K increases. The limit $K\rightarrow\infty$ corresponds to plug flow, i.e., $V(r)$ is independent of r.

For a tube of circular cross section, the ratio of $V_{\max}$ to the mean velocity of the theoretical profile V_{mean} is given by,

$$\frac{V_{\max}}{V_{\text{mean}}}=\frac{\pi R^2}{2\pi\int_0^R rV(r)\mathrm{d}r},$$

for $b=0$ and $a=1$, this can be approximated by

$$\frac{V_{\max}}{V_{\text{mean}}}=\frac{(K+2)}{K}. \tag{2}$$

This ratio is used as an index of the degree of profile blunting; a value of 1 indicates complete plug flow, i.e., all cells moving with the same velocity, and 2 indicates perfect parabolic flow. Fitting Eq. (1) to the experimental data to determine values of K and a was performed using nonlinear curve fitting software (Microcal Origin®) based on the Levenberg-Marquardt algorithm.

3.1.2 *Particle distribution*

The RBC distributions were obtained from DAOCT scans, which, as described earlier, have a contrast derived from the intensity of the peak Doppler-shifted backscattered light. In this case, the intensity of backscattered light from each pixel is governed by the density distribution of RBCs across the tube. On the assumption of a single-backscatter model[13] the measured intensity at each pixel is proportional to the backscattered light intensity from that location attenuated to an extent given by the column integral of the attenuation coefficient of the blood cells from the surface of the tube to the pixel of interest. Because no analytical model has been reported to describe the concentration distribution of red cells such as the tubular pinch effect a polynomial is thus an empirical model. As is standard, the lowest order polynomial consistent with matching the data was used (i.e., the highest order polynomial beyond which the fitting statistics did not improve significantly). To extract the red cell density distribution from the attenuated DAOCT signal a fifth-order polynomial in z^2 (where z is the radial distance across the tube) was used to describe the red cell concentration as a function of depth into the capillary. Using only even powers of z ensures that the model is consistent with the control symmetry of the system. By fitting this model to the experimental data, obtained by averaging several hundred DAOCT scans, parameters describing the red cell density were obtained, from which the distributions could be reconstructed.

The sampling volume is defined as $I_c\times I_x\times I_x$, where I_c is the coherence gate and I_x is the Gaussian beam waist of the sample arm focusing optics.[7] The ASE source and microscope objective used for this investigation produced a sampling volume of 6 pl.

Assuming that the sample volume is small when compared to the diameter of the capillary, the fitting model is described by

$$I(z)=\sigma_B C(z)\exp\left[-2\int_{-R}^{r}\sigma_f C(z)\mathrm{d}z\right], \tag{3}$$

where the constants σ_B and σ_F correspond to the backward- and forward-scattering coefficients of a single RBC. Here $C(z)$ is the fifth-order polynomial in z^2 describing the cell density distribution across the diameter of the tube:

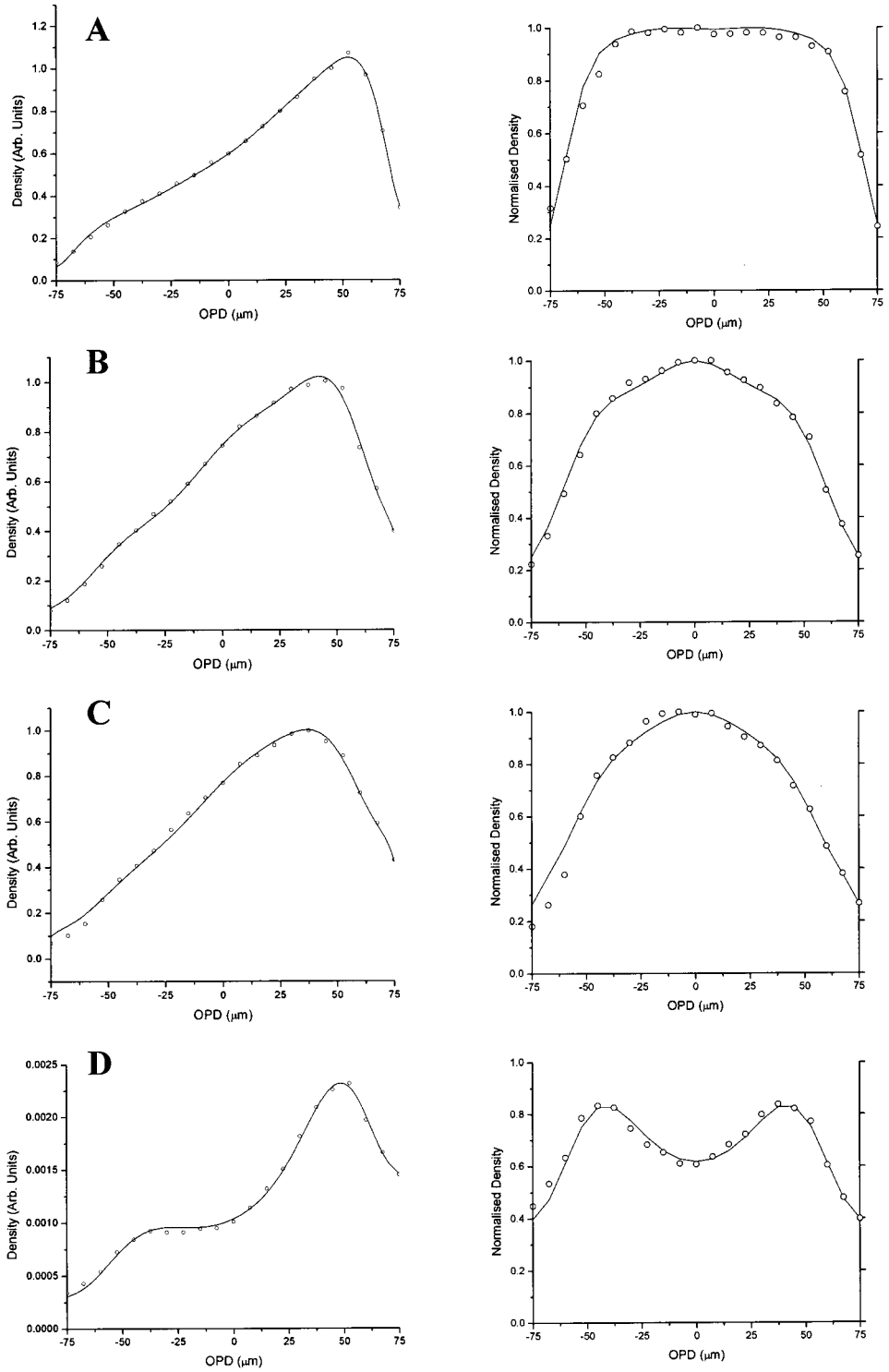

Fig. 11 Left-hand graphs show the raw data points for unfixed RBCs suspended in PBS, obtained by averaging 1000 DAOCT line scans; the polynomial fitting function is shown as a dotted line. The attenuation corrected density distributions are shown on the right-hand side. The four distributions correspond to four flow velocities: (a) 0.5, (b) 6, (c) 12, and (d) 20 mm/s.

$$C(z)=a_0+a_1z^2+a_2z^4+a_3z^6+a_4z^8+a_5z^{10}.$$

Equation (3) was fitted to experimental data generated from an average of 1000 DAOCT line scans through the center of the tube.

4 Results

Measurements were made of velocity profiles and particle concentration distributions as functions of RBC concentration and flow rate for the three types of red cell suspensions in a glass capillary with a diameter of 150 μm.

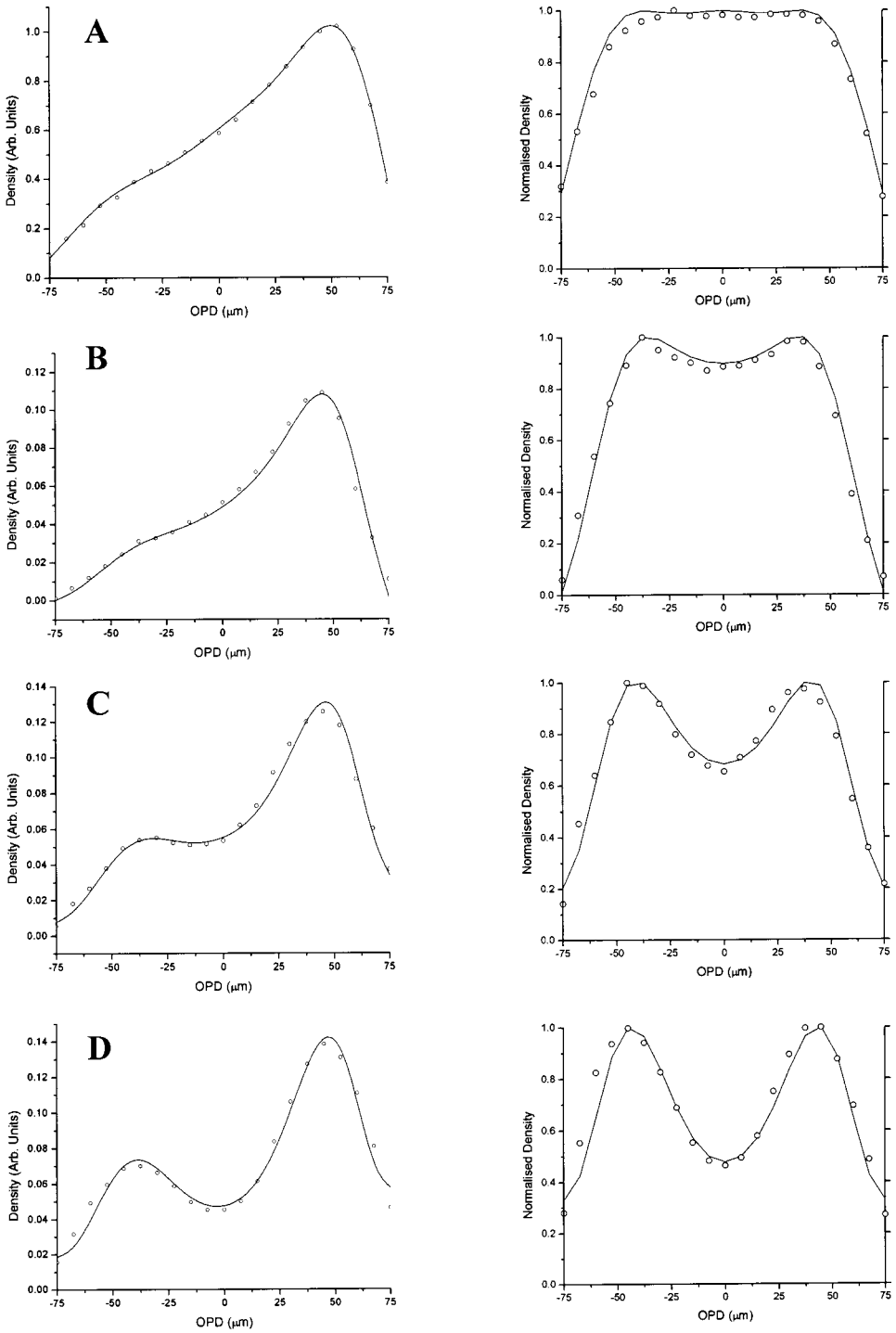

Fig. 12 Left-hand graphs show the raw data points for fixed RBCs suspended in saline, obtained by averaging 1000 DAOCT line scans; the polynomial fitting function is shown as a dotted line. The attenuation corrected density distributions are shown on the right-hand side. The four distributions correspond to four flow velocities; (a) 0.5, (b) 6, (c) 12, and (d) 20 mm/s.

Velocity profiles were obtained for each of the three suspensions at four different flow rates corresponding to mean flow velocities of approximately 0.5, 6, 12, and 20 mm s^{-1}. Results are presented for whole blood and for suspensions of both unfixed and fixed RBCs at concentrations of 40 and 60% by volume. Figures 5–9 show the flow profiles for each solution at the four flow rates. The extent to which the velocity profiles of each solution are blunted as a function of flow rate is quantized by the values of the fitting parameter K, which are summarized in Table 1 along with the associated regression coefficients. The quoted chi-squared values are weighted using the standard error in each pixel calculated from a data set consisting of 1000 line scans through the capillary containing each red cell suspension with average flow velocity of

Table 2 Chi-squared values for the polynomial model of red cell concentration distribution and associated confidence levels p are presented.

	0.5 mm s^{-1}		6.0 mm s^{-1}		12.0 mm s^{-1}		21.0 mm s^{-1}	
	χ^2	p	χ^2	p	χ^2	p	χ^2	p
Fixed	14.1	96.0	13.9	96.3	14.6	95.0	16.0	91.5
Unfixed	13.9	96.4	13.8	96.5	14.5	95.2	13.6	96.3
Whole blood	14.0	96.1	13.5	96.9	13.1	97.5	15.9	91.8

6 mm s^{-1}. The statistical significance of the chi-squared values are described by confidence levels p obtained from confidence level tables for the chi-squared distribution and expressed as percentages.

RBC distribution curves were produced by averaging over 1000 DAOCT line scans. Figures 10–12 show the RBC distributions, before and after attenuation compensation, for whole blood and suspensions of both unfixed and fixed red cells in suspension of 60% by volume. Due to the variation in the backscattered signal intensity of the three suspensions, caused by differing optical properties, the RBC density profiles were normalized to have a peak value of unity. The action of removing the steep background, arising due to the depth-varying attenuation, from the raw data on the left has the effect of enhancing the visibility of noise fluctuations. This causes the distributions on the left column of Figs. 10–12 to appear smoother than those on the right. The regression coefficients of the fitted concentration distributions are presented in Table 2. Again, the statistical significance of the chi-squared values are expressed by confidence levels p shown as percentages.

5 Discussion

The behavior of single particles flowing in suspension through narrow conduits was extensively investigated both experimentally and theoretically. However, describing the complex dynamics of many particles in a concentrated suspension, proved a much more challenging task. The data collected in this study demonstrates the ability of DOCT and DAOCT to provide further insight onto the complex motion arising in concentrated particle suspensions. The velocity profiles obtained at various shear rates for each of the five suspensions agree with the theoretical expectations of departure from Pouseille at low flow rate. All five suspensions showed an increase in the degree of plug flow as shear rates fell. This was most significant in the case of rigid cells, which, as predicted, showed a degree of nonparabolic flow at shear rates significantly higher than the unfixed red cells. Increasing the cell concentration caused both normal and rigid cell suspensions to have a higher degree of plug flow at low shear rates, which was retained to some extent until higher shear rates than for the same suspension at the lower concentration.

The velocity profiles of unfixed RBCs suspended in PBS were sufficiently similar to those of whole blood under the same conditions to assume that the mechanisms controlling the velocity profile of red cells are intrinsic to the cells themselves and are not affected by other components found in whole blood. This supports the assumptions made earlier that red cells are the only components in sufficient concentration to affect significantly the mechanical properties of blood.

The red cell distributions obtained for the three suspensions agree with theoretical expectations, although not quite as closely as the velocity profiles. As predicted, all three solutions show an increasing degree of axial migration as the shear rate is increased, however, not all the suspensions appear to behave as expected.

The fixed red cell suspension exhibits the tubular pinch effect predicted for rigid disks. At the lowest flow rate, the cell distribution is almost uniform apart from a depletion of approximately 20% close to the capillary walls. As the flow velocity and hence shear rate is increased, the depletion region at the walls widens and an area of depletion appears at the capillary center. Increasing the shear rate further exaggerates the areas of depletion until two distinct peaks in cell density are visible with maxima at approximate radii equal to 0.6 of the capillary radius. At the central minimum, the cell density is approximately half that of the maxima.

As in the case of the velocity profiles, the cell distributions of the unfixed red cells suspended in PBS show similar trends to that of whole blood at the same shear rate. At the lowest flow velocity the profiles of both whole blood and the unfixed cell suspension are similar to that of the fixed cell suspension, i.e., uniform apart from a small area of depletion near the capillary wall. As the shear rate is increased the depletion at the capillary wall increases to a maximum of 50% of the maximum value at the center; this behavior can be explained by the axial migration toward the capillary axis predicted for flexible particles. At the highest shear rate, a tubular pinch similar to that of the rigid cells is seen; again the maxima occur at a distance approximately equal to 0.6 the capillary radius from the center, as predicted from theory. This sudden change in cell distribution can be explained by considering the red cell response to shear forces; at very low shear rates below 1 s^{-1}, red cells form rouleaux, which cause an elevated viscosity. At shear rates above 1 to 2 s^{-1}, the rouleaux are broken down and the suspension consists solely of individual cells, which behave as flexible disks able to absorb some of the shear forces in the fluid. At flow rates sufficient to produce shear rates between 10 and 100 s^{-1}, the cells become progressively distorted, hence reducing the viscosity. Once the shear rate reaches approximately 150 s^{-1}, there is a plateau in viscosity; this is due to the cells reaching a maximum com-

pression and behaving as rigid particles, hence exhibiting tubular pinch.[3]

Again, the red cells suspended in PBS show similar flow dynamics to whole blood, reinforcing the assumption that this behavior is intrinsic to the red cells themselves and not a product of the complex makeup of whole blood.

6 Summary

We applied DOCT and a novel variation, DAOCT, to measure both the velocity and concentration profiles of RBCs flowing in a glass capillary tube of diameter 150 μm.

The flow dynamics of red cells are greatly affected by their physical properties. At low flow rates, the velocity profiles and concentration distribution across a narrow capillary can be significantly altered by the rigidity of the cells. Diabetes is known to produce abnormal microcirculation (increased capillary pressure, loss of red cell elasticity, loss of vessel compliance). *In vivo* measurements of red cell distributions could shed light on these processes. At higher flow rates, both normal and rigid cells appear to exhibit identical parabolic flow velocity profiles and both undergo tubular pinch, in which the radial particle concentration distribution becomes peaked at a location from the center equal to 60% of the vessel radius.

The dynamics of red cells in whole blood are the same as those suspended in PBS solution, reinforcing the belief that the red cells are the only component in blood at sufficient concentration to significantly affect its mechanical properties. This also suggests that binding of plasma-based proteins such as albumin to the red cell phospholipid bilayer does not appreciably affect the hydrodynamic properties of the red cell.

References

1. D. W. Slaff, T. J. Arts, and T. G. J. Reneman, ''Electronic measurement of red blood cell velocity and volume flow in microvessels,'' *Invest. Microtech. Med. Biol.* 327–364 (1984).
2. G. J. Tangelder, D. W. Slaff, A. M. M. Muijtjens, T. J. Arts, M. G. A. oude Egbrink, and R. S. Reneman, ''Velocity profiles of blood platelets and red blood cells flowing in arterioles of the rabbit mesentery,'' *Circ. Res.* **59**(5), 505–514 (1986).
3. G. Michelson and B. Schmauss, *Br. J. Ophthamol.* **79**, 1126 (1995).
4. C. G. Caro, T. J. Pedley, R. S. Schroter, and W. A. Seed, *The Mechanics of the Microcirculation*, Oxford Medical Publications, City, (1978).
5. Z. Chen, T. E. Milner, S. Srinivas, X. Wang, A. Malekafzali, M. J. C. van Gemert, and J. S. Nelson, ''Noninvasive imaging of in vivo blood flow velocity using optical Doppler tomography,'' *Opt. Lett.* **22**(14), 1119–1121 (1997).
6. Z. Chen, T. E. Milner, D. D. Dave, and J. S. Nelson, ''Optical Doppler tomographic imaging of fluid flow velocity in highly scattering media,'' *Opt. Lett.* **22**(1), 64–66 (1997).
7. T. G. van Leeuwen, M. D. Kulkarni, S. Yazdanfar, A. M. Rollins, andJ. A. Izatt, ''High-flow-velocity and shear-rate imaging by use of color Doppler optical coherence tomography,'' *Opt. Lett.* **24**(22), 1584–1586 (1999).
8. J. A. Izatt, M. D. Kulkarni, and S. Yazdanfar, ''In-vivo bidirectional color Doppler flow imaging of picoliter blood volumes using optical coherence tomography,'' *Opt. Lett.* **22**(18), 1439–1441 (1997).
9. A. M. Rollins, S. Yazdanfar, J. K. Barton, and J. A. Izatt, ''Real-time in-vivo color Doppler optical coherence tomography,'' *J. Biomed. Opt.* **7**(1), 123–129 (2002).
10. Z. Chen, T. E. Milner, X. Wang, S. Srinivas, and S. J. Nelson, ''Optical Doppler tomography: imaging in vivo blood flow dynamics following pharmacological intervention and photodynamic therapy,'' *Photochem. Photobiol.* **67**, 56–60 (1998).
11. G. J. Tearney, B. E. Bouma, and J. G. Fujimoto, ''High speed phase- and group-delay scanning with a grating based phase control delay line,'' *Opt. Lett.* **22**, 1811–1813 (1997).
12. J. Moger, S. J. Matcher, C. P. Winlove, and A. Shore, ''Measuring blood flow dynamics using DOCT and Doppler amplitude optical coherence tomography (DAOCT),'' in *Coherence Domain Optical Methods in Biomedical Science and Clinical Applications VI*, *Proc. SPIE* **4956**, 366–373 (2003).
13. J. M. Schmitt, A. Knüttel, and R. F. Bonner, ''Measurement of optical properties of biological tissues by low-coherence reflectometry,'' *Appl. Opt.* **32**, 6032–6042 (1993).